Am J Transl Res 2026;18(1):322-335
www.ajtr.org /ISSN:1943-8141/AJTR0169521

Original Article

Comparison of functional recovery between 3D-printed automatic reset splints and traditional fluoroscopy-assisted reduction external fixators in the treatment of tibial shaft fractures

Aorui Yu[1], Kun Gao[2], Mingyu Xiao[3], Yun Zhang[4], Weidong Liu[2]

[1]Department of Traditional Chinese Medicine Orthopaedic Manipulation, Shenzhen Pingle Orthopaedic Hospital Affiliated to Guangzhou University of Traditional Chinese Medicine, Shenzhen 518118, Guangdong, China; [2]Department of Orthopaedics, Shenzhen Traditional Chinese Medicine Hospital Affiliated to Guangzhou University of Traditional Chinese Medicine, Shenzhen 518033, Guangdong, China; [3]Fifth Department of Orthopedics, Laizhou Hospital of Traditional Chinese Medicine, Yantai 261400, Shandong, China; [4]Department of Medical Quality Control, Shenzhen Pingle Orthopaedic Hospital Affiliated to Guangzhou University of Traditional Chinese Medicine, Shenzhen 518118, Guangdong, China

Received October 24, 2025; Accepted December 22, 2025; Epub January 15, 2026; Published January 30, 2026

Abstract: Objectives: Tibial shaft fractures are common yet challenging to manage, with external fixation being a standard approach. This study aimed to compare functional recovery between two reduction and fixation techniques: traditional fluoroscopy-assisted external fixators and novel 3D-printed automatic reset splints. Methods: A retrospective analysis included 193 patients with open tibial shaft fractures treated between January 2021 and December 2024. Participants were divided into a traditional fluoroscopy-assisted (TF-A) group (n=104) and a 3D-printed automatic reset splint (3D-P) group (n=89). Reduction effectiveness was assessed using radiographic measurements (X, α, Y, Z, β) preoperatively and at 1 week, 1 month, 3months, and 6 months postoperatively. Healing status (callus formation and healing time), treatment efficacy, complication rates, knee function (HSS score), and pain intensity (VAS score) were evaluated during a 6-month follow-up. Results: The 3D-P group demonstrated significantly better reduction across most deformity parameters (e.g., 1-week Y: 2.43±0.78 mm vs. 2.76±0.86 mm, P=0.006), shorter callus formation time (16.84±3.12 vs. 18.49±4.28 days, P=0.002), and faster fracture healing (72.97±10.93 vs. 78.26±15.33 days, P=0.006). Excellent efficacy rates were higher (69.66% vs. 51.92%, P=0.012), and total complications lower (20.22% vs. 33.65%, P=0.037). The 3D-P group also had superior knee function (HSS: 86.62±6.44 vs. 84.33±5.39, P=0.008) and lower pain VAS scores at all postoperative timepoints (e.g., 1 week: 4.93±0.86 vs. 5.37±1.02, P=0.002). Conclusions: Three-dimensional printed automatic reset splints offer significant advantages over traditional fluoroscopy-assisted fixation in improving reduction accuracy, accelerating healing, reducing complications, and enhancing functional recovery in tibial shaft fractures.

Keywords: 3D printing, external fixators, tibial fractures, fracture fixation, rehabilitation

Introduction

Tibial shaft fractures represent a significant clinical challenge in orthopedic trauma, constituting approximately 2% of all fractures and often resulting from high-energy mechanisms such as traffic accidents or falls from height [1, 2]. The management of these injuries, particularly open fractures, is complex due to the precarious soft tissue envelope, limited vascular supply, and high mechanical demands placed on the tibia. The primary treatment objectives are to achieve anatomical reduction, provide stable fixation, preserve biological viability, and facilitate early functional rehabilitation-all of which are critical for restoring limb function and preventing long-term disability [3, 4].

External fixation has long been a cornerstone in the initial and in some cases, definitive management of open tibial shaft fractures, especially in situations with substantial soft tissue

https://doi.org/10.62347/OAEI5930

compromise [5, 6]. Traditional fluoroscopy-assisted (TF-A) reduction and external fixation offers the advantages of being minimally invasive and providing adjustable stability. However, this technique relies heavily on intraoperative two-dimensional imaging, which can lead to suboptimal reduction accuracy, increased radiation exposure, and prolonged operative time. Imperfect reduction may contribute to malunion, delayed healing, and altered biomechanics, ultimately compromising functional outcomes [7, 8].

The inherent limitations of conventional methods have spurred the exploration of advanced technologies for improved fracture care. The integration of three-dimensional (3D) printing technology represents a paradigm shift toward personalized and precision medicine in orthopedics [9, 10]. This approach involves acquiring preoperative computed tomography (CT) data of the affected limb, performing a virtual reduction in a digital environment, and then using computer-aided design (CAD) to create a patient-specific external fixation splint that mirrors the individual's anatomy and the reduced fracture position [11, 12]. This customized splint is then manufactured using 3D printing.

This innovative workflow potentially addresses several key limitations of traditional methods. First, regarding precision and stability, by translating a precise preoperative virtual plan into physical reality, 3D-printed splints may achieve superior fracture reduction accuracy and maintain it more consistently, thereby minimizing intraoperative guesswork [13]. Second, concerning biological benefits, the personalized design that accounts for soft tissue contours may minimize iatrogenic soft tissue damage and better preserve the vascular supply, creating a more favorable biological environment for bone healing [13, 14]. Third, in terms of clinical outcomes, the improved stability and biological respect could translate into faster healing rates, reduced risks of complications such as infection and malunion, and enhanced functional recovery [10, 13]. It is within this context of addressing persistent challenges in tibial fracture management that this study was conceived, aiming to evaluate whether this novel 3D-printed automatic reset splint translates into superior functional recovery compared to traditional fluoroscopy-assisted external fixation.

Materials and methods

Selection criteria

A retrospective analysis was conducted on 193 patients with tibial shaft fractures admitted to Shenzhen Pingle Orthopaedic Hospital Affiliated to Guangzhou University of Traditional Chinese Medicine from January 2021 to December 2024. Inclusion criteria: ① Age between 18 and 70 years; ② Clinically diagnosed with unilateral tibial shaft open fracture [15]; ③ Gustilo classification [16] of type II or IIIA; ④ AO Foundation [17] classification of type A or B; ⑤ Time from injury to treatment <10 days; ⑥ Complete medical records without any missing data. Exclusion criteria: ① Old fractures, pathological fractures, severely comminuted fractures, or fractures that are difficult to accurately reduce; ② Concomitant fractures or joint dislocations in other parts of the same lower limb; ③ Previous history of lower limb fractures, deformities, fracture surgeries, or orthopedic surgeries on either side; ④ Systemic diseases affecting fracture healing; ⑤ Nerve injuries or vascular injuries; ⑥ Follow-up period <6 months.

This retrospective study was conducted in accordance with the ethical principles of the Declaration of Helsinki and was approved by the ethics committee of Shenzhen Pingle Orthopaedic Hospital Affiliated to Guangzhou University of Traditional Chinese Medicine. The need for informed consent was waived by the ethics committee due to the retrospective nature of the study.

Grouping criteria

Based on different external fixation treatment methods, 193 eligible patients with open tibial shaft fractures were divided into two groups: the traditional fluoroscopy-assisted (TF-A) group (n=104) and the 3D-printed (3D-P) group (n=89). Patients in the TF-A group received reduction and fixation treatment using a traditional external fixator assisted by C-arm X-ray fluoroscopy, while patients in the 3D-P group received treatment with a 3D-printed automatic reset external fixation splint based on preoperative CT three-dimensional reconstruction. All surgeries were performed by the same physician with over five years of experience in external fixation treatment for tibial shaft fractures.

Treatment process

Traditional fluoroscopy-assisted reduction external fixators: For patients in the TF-A group, they were placed in a supine position, and the operating table was adjusted to ensure patient comfort and easy exposure of the surgical site. An inflatable tourniquet was applied to the root of the affected thigh. After successful general anesthesia, open wounds were thoroughly disinfected and debrided, and suturable wounds were closed. Non-suturable wounds were covered with negative pressure wound therapy. Anteromedial or anterolateral incisions were made, with 5 cm incisions above and below the fracture site to expose the fracture ends by cutting through the skin and subcutaneous tissue. Reduction was assisted using reduction clamps and bone levers under fluoroscopic guidance provided by a C-arm X-ray machine (Cstar, Hangzhou MeNowa Medical Technology Co., Ltd., China), aiming to restore the original axis and length of the tibia as much as possible. After reduction, an external fixator was applied.

A 4 mm diameter K-wire was drilled into the cortical bone segment. Initially, the bilateral external fixation rods were fixed, then two distant K-wires at the proximal and distal ends were connected for fracture reduction. Additional K-wires were inserted 3-4 cm from the fracture ends at both the proximal and distal sites. The position of the fixator was adjusted to ensure proper alignment of the fracture ends, and screws were used to secure the proximal and distal segments. Upon completion of the surgery, the wound was thoroughly examined to ensure there was no active bleeding or other abnormalities, cleaned, and closed using absorbable sutures for continuous suturing of the subcutaneous tissue and skin.

3D-printed automatic reset splints: (1) Patient's CT 3D reconstruction: Preoperative scans of the affected limb and the contralateral healthy limb were performed using a CT scanner (SOMATOM Definition Flash, Siemens, Germany). The scanning parameters were set as follows: slice thickness (0.625 mm); voltage (120 kV); current (300 mA). The acquired Digital Imaging and Communications in Medicine (DICOM) files were imported into Mimics software v19.0 (Materialise, Leuven, Belgium). Using functions such as "threshold segmentation" and "layer editing", images of external fixation pins, bones, and skin contours were segmented (thresholds set at >2500 HU, 500-2000 HU, and <300 HU, respectively), and then 3D reconstructions were sequentially performed using the software's "3D reconstruction" feature.

(2) Virtual reduction: Under the guidance of an orthopedic surgeon, the "translation" and "rotation" functions of Mimics v19.0 were used to move the distal bone segment (along with its external fixation pins) so that the fracture surfaces aligned with those of the proximal segment, completing the virtual reduction. When the fracture site had multiple fragments or bone defects, making it difficult to align based on surface details, the healthy-side bone was mirrored and used as a template for fracture reduction.

(3) Design and manufacturing of 3D printed automatic reduction external fixation splints: The 3D images of skin contours, reduced bones, and external fixation pins were exported from Mimics 19.0 software as STL files and then imported into SolidWorks 2014 software for assembly. Soft tissue injury sites were marked on the skin contour. Based on the anticipated postoperative swelling, the skin contour was expanded by an appropriate distance (typically 3 mm) and thickened by 5 mm to form the prototype of the 3D printed automatic reduction external fixation splint. Corresponding fixation holes and pressure pads were designed according to the positions of the external fixation pins. The scaffold was divided into four parts based on the positions of the fixation holes, followed by optimization designs such as hollowing, cutting, reinforcing, and drilling. Finally, the exposed heights of the external fixation pins on the scaffold were recorded, or corresponding height detection rulers were designed. The designed scaffold in SolidWorks 2014 was exported as an STL file, then imported into 3D printing software (Cura software v15.02) for pose adjustment, automatic layering, and support structure generation. The generated data were then transmitted to a 3D printer (3D ORTHO Waston Med Co., Ltd., Changzhou, Jiangsu, China). After printing, the support structures were removed, and post-processing such as polishing and cleaning was performed.

Figure 1. Lateral X-ray of a typical case in TF-A group. A. Pre-operative lateral X-ray showed fracture lines; B. Lateral X-ray at 1 day after external fixator fixation showed the external fixator needle was correctly placed, fracture end was stable and fixed, and fracture end was well aligned. TF-A, Traditional Fluoroscopy-Assisted.

(4) Surgical execution based on virtual reduction plan: After removing the temporary external fixator, the affected limb was placed into a sterilized 3D-printed automated reduction external fixator. First, the proximal external fixation pins were inserted into the corresponding fixing holes at the proximal end of the fixator and preliminarily tightened after adjusting their exposed height to a predetermined value using a pre-designed height detection ruler. At this stage, the fixator ensured the accuracy of the proximal screw positions. Subsequently, traction was applied along the axial direction of the limb. During traction, changes in the soft tissue tension of the affected limb guided the distal bone segment's movement according to the inner surface morphology of the fixator. The personalized three-dimensional structure of the fixator played an "automatic reduction" role at this moment, passively guiding the distal bone fragment to the anatomical position predetermined by the virtual plan. Next, the distal external fixation pins were slid into the corresponding fixing holes at the distal end of the fixator. After ensuring the accurate positioning and height adjustment of both proximal and distal pins, connecting rods and clamps were used to securely connect all external fixation pins into a complete rigid frame. Finally, fluoroscopy was performed using a C-arm X-ray machine (Cstar, Hangzhou MeNowa Medical Technology Co., Ltd., China) to confirm the consistency between the fracture reduction effect and the virtual plan.

Postoperative care: All patients received the following routine external fixation care postoperatively: (1) The needle insertion sites were disinfected 2 to 3 times a day using medical alcohol; (2) Dressings were changed regularly based on soft tissue healing status (if there was no significant exudate, dressing changes were not necessary); (3) The fixation screws of the external fixator were checked regularly to prevent loosening; (4) Patients with satisfactory reduction and stable fixation were allowed to perform non-weight-bearing joint functional exercises postoperatively; (5) Partial weight-bearing was permitted 1 week postoperatively.

Function recovery indicators

The primary outcome measures of this study were reduction effectiveness, postoperative healing status, efficacy evaluation, and incidence of complications. The secondary outcome measures were knee function scores and pain intensity scores. All patients completed a 6-month follow-up period.

(1) Reset effect: Preoperative and at 1 week, 1 month, 3 months, and 6 months postoperative, anteroposterior and lateral radiographs of the tibial fracture specimens were taken to measure the following deformity parameters: mediolateral displacement (X), mediolateral angulation (α), axial displacement (Y), antero-

Figure 2. Lateral X-ray of a typical case in 3D-P group. A. Pre-operative lateral X-ray showed the fracture line and fracture fragment was misaligned; B. Lateral X-ray at 1 day after external fixation surgery showed that the external fixator pins were correctly positioned, providing stable fixation of the fracture ends with good alignment. 3D-P, 3D-Printed.

posterior displacement (Z), and anteroposterior angulation (β). X was the maximum perpendicular distance between the fractured fragments in the coronal plane. α was the angle of deformity in the coronal plane, measured as the angle between the longitudinal axes of the proximal and distal main fragments. Y was the maximum shortening or overriding of the fracture fragments along the long axis of the tibia. Z was the maximum perpendicular distance between the fractured fragments in the sagittal plane. β was the angle of deformity in the sagittal plane, measured as the angle between the longitudinal axes of the proximal and distal main fragments (**Figures 1** and **2**).

(2) Postoperative Healing Status: Bone callus formation and fracture healing time were assessed according to the criteria outlined in the "Chinese Guidelines for Diagnosis and Treatment of Open Fractures (2019 Edition)" [15]. Bone callus formation was determined by the following signs: blurred fracture lines, reduced soft tissue swelling, and the appearance of sclerotic borders around the fracture site on X-ray. The criteria for fracture healing included: absence of longitudinal percussion pain, tenderness, or abnormal movement at the fracture site; blurred fracture lines with continuous bone callus observed on X-rays; ability to lift a 1 kg weight forward for 1 minute with the upper limb after removal of external fixation, or continuous walking for 3 minutes and ≥30 steps on flat ground with the lower limb; and no change in fracture stability over a continuous observation period of 2 weeks.

(3) Efficacy evaluation: The study adopted the commonly used domestic criteria for evaluating the efficacy of long bone fracture treatment (see **Table 1**).

(4) Incidence of complications: The occurrence of complications, including superficial infection, deep infection, pin tract infection, malunion, and nonunion, were observed and compared during the follow-up period. Infection-related conditions were a key focus of this study. Superficial infections were defined as infections involving the skin and subcutaneous tissues around the needle tract or surgical incision, characterized by local redness, swelling, heat, pain, and purulent discharge. Deep infections were defined as infections that involve the deep fascia, muscles, or bone tissue, potentially accompanied by systemic infection symptoms (such as fever), and confirmed through imaging studies (e.g., X-rays showing bone destruction) or pathogen culture. Pin tract infections were defined as bacterial infections occurring at the interface between the needle and the skin, forming a channel (i.e., "needle tract"). The diagnosis of all infection events was based on a combination of clinical signs, laboratory tests, and imaging assessments.

Table 1. Criteria for evaluating the efficacy of long bone fracture treatment in China

	Joint Activity	Pain	Angular Deformity	Shortening Deformity
Excellent	Normal range of motion restored	None	None	<1 cm
Good	Motion restricted by <50%	Occasional	None	<2 cm
General	Motion restricted by >50%	Frequent	<10°	<3 cm

(5) Knee function scores: The Hospital for Special Surgery (HSS) scoring system was used to compare knee function scores between the two groups at preoperative and 6 months postoperative. The HSS score evaluates pain, function, range of motion, muscle strength, and other aspects, with a total score of 100 points; higher scores indicate better knee function in patients. The Cronbach's alpha for this scale is 0.87 [18].

(6) Pain intensity scores: The Visual Analog Scale (VAS) was utilized to assess the pain intensity of patients in both groups at preoperative, 1 week, 1 month, 3 months, and 6 months postoperative. The VAS score ranges from 0 to 10, with higher scores indicating more severe pain. The intraclass correlation coefficient for test-retest reliability of this scale ranges from 0.97 to 0.99 [19].

Statistics

In this study, statistical analyses were performed using SPSS software (Version 29.0; developed by SPSS Inc., Chicago, IL, USA). Continuous variables were assessed for normality using the Shapiro-Wilk test and were reported as means ± standard deviations (means ± SD) since they met the criteria for normal distribution. For comparisons between groups, independent samples t-tests were employed. Categorical variables were presented as frequencies and percentages [n (%)] and were compared between groups using the chi-square test. The significance level was set at α=0.05.

Results

Basic data

In comparing the demographic characteristics between the TF-A group (n=104) and the 3D-P group (n=89), our results indicated no significant differences in age, gender distribution, BMI, insurance type, educational background, occupational type, marital status, smoking history, drinking history, hypertension, and diabetes between the two groups (all P>0.05). These findings suggest that the baseline demographic characteristics were well balanced across the treatment groups, ensuring comparability for further analysis on functional recovery outcomes (**Table 2**).

In the comparison of fracture features between the TF-A group and the 3D-P group, no significant differences were observed across various parameters. There were no significant differences in the cause of fracture, site of fracture, side of fracture, type of fracture, AO classification, Gustilo classification, soft tissue defect size, and time from injury to operation between the two groups (all P>0.05). These results indicate that the baseline fracture characteristics were similar between the two treatment groups, supporting comparability for further analysis on the effectiveness of the treatments (**Table 3**).

Reset effect

When evaluating the reset effect between the TF-A group and the 3D-P group, several parameters showed significant differences postoperatively. Preoperative measurements for all parameters (X, α, Y, Z, β) did not show any significant differences between the two groups (all P>0.05). For X (Medial-Lateral Displacement), there were significant differences at 1 week (P=0.003), 1 month (P=0.015), 3 months (P=0.018), but not at 6 months (P>0.05). For α (Medial-Lateral Angulation), significant differences were noted at 1 week (P=0.021), 1 month (P=0.023), 3 months (P=0.021), and 6 months (P=0.021). Y (Axial Displacement) showed significant differences at 1 week (P=0.006), 1 month (P=0.011), 3 months (P=0.040), and 6 months (P=0.047). Z (Anterior-Posterior Displacement) demonstrated significant differences at 1 week (P=0.013), 1 month (P=0.016), 3 months (P=0.019), but not at 6 months (P>0.05). For β (Anterior-Posterior Angulation), significant differences were ob-

Table 2. Comparison of demographic characteristics between two groups

Parameter	TF-A group (n=104)	3D-P group (n=89)	t/χ^2	P
Age (years)	41.75±8.36	40.92±8.51	0.683	0.495
Gender [n (%)]			0.638	0.424
Male	70 (67.31%)	55 (61.80%)		
Female	34 (32.69%)	34 (38.20%)		
BMI (kg/m^2)	23.22±2.15	23.27±2.19	0.150	0.881
Insurance type [n (%)]			0.729	0.694
Urban insurance	62 (59.62%)	48 (53.93%)		
Rural medical insurance	30 (28.85%)	28 (31.46%)		
Self-payment	12 (11.54%)	13 (14.61%)		
Educational background [n (%)]			1.019	0.601
Junior high or below	38 (36.54%)	27 (30.34%)		
High school	45 (43.27%)	40 (44.94%)		
Tertiary and above	21 (20.19%)	22 (24.72%)		
Occupational type [n (%)]			0.796	0.372
Manual labor	65 (62.50%)	50 (56.18%)		
Mental labor	39 (37.50%)	39 (43.82%)		
Marital status [n (%)]			0.679	0.712
Married	72 (69.23%)	57 (64.04%)		
Single	25 (24.04%)	26 (29.21%)		
Divorced/Widowed	7 (6.73%)	6 (6.74%)		
Smoking history [n (%)]			0.232	0.630
Yes	48 (46.15%)	38 (42.70%)		
No	56 (53.85%)	51 (57.30%)		
Drinking history [n (%)]			0.039	0.843
Yes	40 (38.46%)	33 (37.08%)		
No	64 (61.54%)	56 (62.92%)		
Hypertension [n(%)]			0.001	0.974
Yes	22 (21.15%)	19 (21.35%)		
No	82 (78.85%)	70 (78.65%)		
Diabetes [n (%)]			0.175	0.676
Yes	15 (14.42%)	11 (12.36%)		
No	89 (85.58%)	78 (87.64%)		

Notes: TF-A, Traditional Fluoroscopy-Assisted; 3D-P, 3D-Printed; BMI, Body Mass Index.

served at 1 week (P=0.008), 1 month (P=0.018), 3 months (P=0.045), and 6 months (P=0.039). These results indicate that the 3D-printed automatic resetting splints provided a significantly better reset effect compared to traditional fluoroscopy-assisted external fixation during the early stages of recovery, with sustained improvements over time (**Table 4**).

Postoperative healing status

In evaluating the postoperative healing status between the TF-A group and the 3D-P group, significant differences were observed in both the time to callus formation and fracture healing time. The time to callus formation was significantly shorter in the 3D-P group compared to the TF-A group (P=0.002). Similarly, the fracture healing time was also significantly reduced in the 3D-P group (P=0.006). These results suggest that the use of 3D-printed automatic resetting splints is associated with a faster healing process, including quicker callus formation and overall fracture healing, compared to traditional fluoroscopy-assisted external fixation (**Figure 3**).

Efficacy evaluation

In the comparison of efficacy evaluation between the TF-A group and the 3D-P group, sig-

Table 3. Comparison of fracture features between two groups

Parameter	TF-A group (n=104)	3D-P group (n=89)	t/χ^2	P
Cause of fracture [n (%)]			1.687	0.640
Traffic accident injuries	58 (55.77%)	46 (51.69%)		
Fall from height injuries	30 (28.85%)	23 (25.84%)		
Mechanical injuries	13 (12.50%)	17 (19.10%)		
Other causes	3 (2.88%)	3 (3.37%)		
Site of fracture [n (%)]			0.357	0.836
Upper	25 (24.04%)	20 (22.47%)		
Middle	40 (38.46%)	38 (42.70%)		
Lower	39 (37.50%)	31 (34.83%)		
Side of fracture [n (%)]			0.635	0.426
Left	48 (46.15%)	36 (40.45%)		
Right	56 (53.85%)	53 (59.55%)		
Type of fracture [n (%)]			0.220	0.896
Transverse	45 (43.27%)	36 (40.45%)		
Oblique	32 (30.77%)	30 (33.71%)		
Spiral	27 (25.96%)	23 (25.84%)		
AO classification [n (%)]			0.015	0.903
A	57 (54.81%)	48 (53.93%)		
B	47 (45.19%)	41 (46.07%)		
Gustilo classification [n (%)]			0.092	0.762
II	63 (60.58%)	52 (58.43%)		
III A	41 (39.42%)	37 (41.57%)		
Soft tissue defect (cm^2)	5.32±1.25	5.28±1.31	0.207	0.837
Time from injury to operation (days)	4.28±0.76	4.35±0.88	0.591	0.555

Notes: TF-A, Traditional Fluoroscopy-Assisted; 3D-P, 3D-Printed; AO, AO Foundation.

nificant differences were observed in the distribution of outcomes. The 3D-P group had a significantly higher proportion of patients achieving an "excellent" outcome compared to the TF-A group (P=0.012). There was no significant difference in the proportion of patients achieving a "good" outcome or a "general" outcome (all P>0.05) between the two groups. These findings indicate that the use of 3D-printed automatic resetting splints is associated with a higher rate of excellent treatment outcomes compared to traditional fluoroscopy-assisted external fixation, suggesting potential advantages of this advanced technology in improving overall treatment efficacy (**Table 5**).

Incidence of complications

In the comparison of complications incidence rates between the TF-A group and the 3D-P group, the total complication rate was significantly lower in the 3D-P group compared to the TF-A group (20.22% vs 33.65%, χ^2=4.342, P=0.037). Specifically, there were fewer cases of superficial infection (6.74% vs 14.42%), deep infection (1.12% vs 4.81%), pin tract infection (10.11% vs 19.23%), malunion (4.49% vs 12.50%), and nonunion (2.25% vs 6.73%) in the 3D-P group, although individual complication rates did not reach statistical significance on their own. These results suggest that the use of 3D-printed automatic resetting splints is associated with a reduced overall incidence of postoperative complications compared to traditional fluoroscopy-assisted external fixation. This indicates that using advanced 3D printing technology has the potential to reduce the risk of various complications, including infection, after the treatment of tibial shaft fractures (**Table 6**).

Knee joint function score

In the comparison of knee joint function scores between the TF-A group and the 3D-P group, significant differences were observed in sever-

Table 4. Comparison of reset effect between two groups

Parameter	TF-A group (n=104)	3D-P group (n=89)	t	P
X (mm)				
Preoperatively	8.52±2.31	8.47±2.28	0.151	0.880
1 week postoperatively	3.35±0.98	2.95±0.86	3.002	0.003
1 month postoperatively	3.13±0.95	2.82±0.83	2.442	0.015
3 months postoperatively	3.05±0.92	2.77±0.71	2.377	0.018
6 months postoperatively	2.92±0.73	2.75±0.66	1.593	0.113
α (°)				
Preoperatively	12.35±3.42	12.28±3.38	0.138	0.891
1 week postoperatively	5.43±1.75	4.87±1.56	2.335	0.021
1 month postoperatively	5.27±1.62	4.76±1.44	2.299	0.023
3 months postoperatively	5.19±1.48	4.72±1.31	2.325	0.021
6 months postoperatively	5.07±1.33	4.65±1.19	2.326	0.021
Y (mm)				
Preoperatively	7.25±2.12	7.18±2.09	0.234	0.815
1 week postoperatively	2.76±0.86	2.43±0.78	2.798	0.006
1 month postoperatively	2.62±0.84	2.32±0.76	2.563	0.011
3 months postoperatively	2.48±0.75	2.26±0.71	2.07	0.040
6 months postoperatively	2.45±0.74	2.25±0.66	2.002	0.047
Z (mm)				
Preoperatively	7.92±2.28	7.87±2.25	0.150	0.881
1 week postoperatively	3.09±0.92	2.76±0.88	2.507	0.013
1 month postoperatively	2.92±0.88	2.62±0.84	2.436	0.016
3 months postoperatively	2.87±0.85	2.58±0.82	2.368	0.019
6 months postoperatively	2.74±0.82	2.54±0.79	1.774	0.078
β (°)				
Preoperatively	11.25±3.17	11.18±3.15	0.145	0.885
1 week postoperatively	4.47±1.43	3.95±1.26	2.665	0.008
1 month postoperatively	4.34±1.41	3.88±1.24	2.386	0.018
3 months postoperatively	4.31±1.32	3.94±1.22	2.017	0.045
6 months postoperatively	4.16±1.27	3.79±1.15	2.077	0.039

Notes: TF-A, Traditional Fluoroscopy-Assisted; 3D-P, 3D-Printed; X, Medial-Lateral Displacement; α, Medial-Lateral Angulation; Y, Axial Displacement; Z, Anterior-Posterior Displacement; β, Anterior-Posterior Angulation.

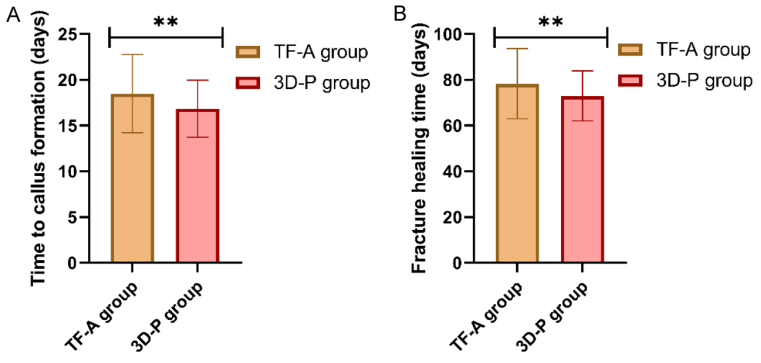

Figure 3. Comparison of postoperative healing status between two groups (days). Notes: TF-A, Traditional Fluoroscopy-Assisted; 3D-P, 3D-Printed; **: P<0.01.

al parameters at the 6-month postoperative evaluation. Preoperative scores for pain, function, range of motion, muscle strength, and total score did not show any significant differences between the two groups (all P>0.05). For pain, there was a significant difference favoring the 3D-P group (P= 0.006). Function scores also showed a significant improvement in the 3D-P group compared to the TF-A group (P= 0.001). The range of motion

Table 5. Comparison of efficacy evaluation between two groups [n (%)]

Parameter	TF-A group (n=104)	3D-P group (n=89)	χ^2	P
Excellent	54 (51.92%)	62 (69.66%)	6.294	0.012
Good	38 (36.54%)	22 (24.72%)	3.127	0.077
General	12 (11.54%)	5 (5.62%)	2.093	0.148

Notes: TF-A, Traditional Fluoroscopy-Assisted; 3D-P, 3D-Printed.

Table 6. Comparison of complications incidence rates between two groups [n (%)]

Parameter	TF-A group (n=104)	3D-P group (n=89)	χ^2	P
Total complication rate	35 (33.65%)	18 (20.22%)	4.342	0.037
Superficial infection	15 (14.42%)	6 (6.74%)		
Deep infection	5 (4.81%)	1 (1.12%)		
Pin tract infection	20 (19.23%)	9 (10.11%)		
Malunion	13 (12.50%)	4 (4.49%)		
Nonunion	7 (6.73%)	2 (2.25%)		

Notes: TF-A, Traditional Fluoroscopy-Assisted; 3D-P, 3D-Printed.

demonstrated a significant difference at 6 months postoperatively (P=0.018). Muscle strength scores were significantly higher in the 3D-P group at 6 months postoperatively (P=0.016). Finally, the total knee joint function score was significantly better in the 3D-P group compared to the TF-A group at 6 months postoperatively (P=0.008). These results indicate that the use of 3D-printed automatic resetting splints is associated with better knee joint functional recovery at 6 months postoperatively compared to traditional fluoroscopy-assisted external fixation (**Table 7**).

Pain level score

In the comparison of pain level scores between the TF-A group (n=104) and the 3D-P group (n=89), significant differences were observed at various postoperative time points. Preoperatively, there was no significant difference in pain levels between the two groups (P>0.05). However, starting from 1 week postoperatively, the 3D-P group showed significantly lower pain scores compared to the TF-A group: 1 week (P=0.002), 1 month (P=0.003), 3 months (P=0.011), and 6 months (P=0.029). These results indicate that patients treated with 3D-printed automatic resetting splints experienced significantly less pain throughout the recovery period compared to those treated with traditional fluoroscopy-assisted external fixation. The consistent reduction in pain scores suggests that the use of advanced 3D-printed technology may contribute to better pain management and improved patient comfort following tibial shaft fracture treatment (**Figure 4**).

Discussion

This comparative study demonstrates that the use of 3D-printed automatic reset splints for the management of open tibial shaft fractures leads to improved functional recovery outcomes across multiple domains when compared to traditional fluoroscopy-assisted external fixation. The observed differences in reduction quality, healing parameters, complication rates, knee function, and pain levels collectively suggest that this innovative approach offers tangible clinical benefits.

The 3D-printed group demonstrated significantly better radiographic alignment across most parameters throughout recovery. This underscores the core technical advantage of the technology that the seamless translation of a preoperative virtual plan into physical reality. This finding strongly aligns with previous investigations into computer-assisted design and 3D printing in fracture management [20, 21]. As Shin et al. suggested, the ability to simulate reduction digitally and create a patient-specific device that guides anatomical realignment minimizes the intraoperative guesswork and extensive radiation exposure inherent in traditional methods, which rely heavily on two-dimensional fluoroscopic imaging and surgeon experience [21]. Our results demonstrate that this paradigm shift, from intraoperative trial-and-error to preoperative precision planning, directly translates to superior and sustained fracture reduction. The consistent maintenance of reduction over time further suggests that 3D-printed splints provide a more stable mechanical environment, which is a critical determinant for long-term functional outcomes and lower extremity biomechanics [22, 23].

Table 7. Comparison of knee joint function score between two groups (points)

Parameter	TF-A group (n=104)	3D-P group (n=89)	t	P
Pain				
Preoperatively	17.56±4.83	18.85±4.67	1.864	0.064
6 months postoperatively	23.03±4.48	24.92±4.84	2.807	0.006
Function				
Preoperatively	12.06±2.35	11.45±2.37	1.784	0.076
6 months postoperatively	18.13±2.96	19.71±3.65	3.276	0.001
Range of motion				
Preoperatively	8.74±1.98	8.92±2.03	0.607	0.545
6 months postoperatively	15.11±4.35	16.52±3.74	2.385	0.018
Muscle strength				
Preoperatively	6.08±1.16	5.85±1.04	1.410	0.160
6 months postoperatively	8.39±1.63	8.97±1.71	2.425	0.016
Total score				
Preoperatively	54.42±7.88	55.69±8.13	1.101	0.272
6 months postoperatively	84.33±5.39	86.62±6.44	2.688	0.008

Notes: TF-A, Traditional Fluoroscopy-Assisted; 3D-P, 3D-Printed.

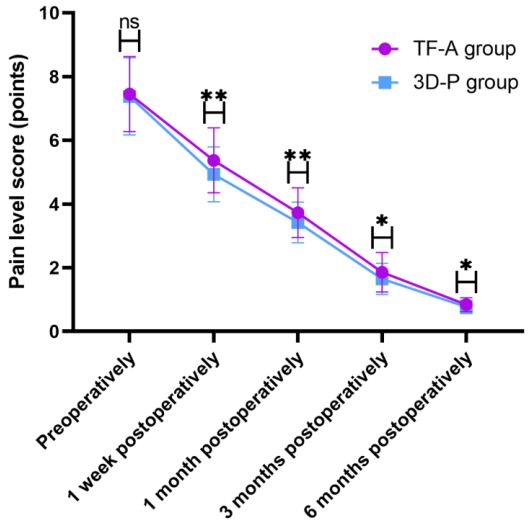

Figure 4. Comparison of Pain level score between two groups (points). Notes: TF-A, Traditional Fluoroscopy-Assisted; 3D-P, 3D-Printed; ns: no significant difference; *: P<0.05; **: P<0.01.

Our findings indicating accelerated callus formation and shorter overall fracture healing time in the 3D-printed group suggest a positive influence on the biological aspects of fracture repair. This biological advantage can be attributed to the minimally invasive and personalized nature of the 3D-printed approach, as supported by previous reports [24, 25]. The customized design, which accounts for individual anatomy and anticipated soft tissue swelling, minimizes iatrogenic soft tissue disruption and better preserves the precarious vascular supply around the tibia, a factor crucial for bone regeneration [24]. Furthermore, studies have indicated that 3D-printed orthopedic devices can be engineered to optimize the mechanical microenvironment. For instance, Li et al. highlighted that customized fixation can optimize interfragmentary strain to levels more conducive to efficient callus formation [24]. This combination of biological respect and mechanical optimization likely creates an ideal milieu for healing, explaining the significantly faster recovery times observed in our study [26].

The significantly lower overall complication rate observed with 3D-printed splints, particularly concerning pin tract infections and malunion, represents a clinically critical advancement. This reduction aligns with the findings of Qiao et al., who reported that patient-specific contouring and precise pre-planned pin placement minimize soft tissue irritation and pressure points, thereby enhancing tissue viability and reducing the risk of infection [25]. Traditional external fixators, with their standardized components, often exert uneven pressure, leading to skin necrosis and pin loosening. In contrast, the improved initial reduction and stability provided by the 3D-printed splint decrease mechanical stress on the fixation pins, reducing the primary cause of pin loosening and sub-

sequent infection [27]. The marked reduction in malunion cases specifically validates the ability of personalized splints to maintain anatomical alignment, potentially preventing the need for corrective surgeries and their associated morbidity, as discussed in other reports on malunion treatment [28].

The superior knee function recovery and consistently lower pain levels in the 3D-printed group highlight the ultimate goal of fracture treatment: restoring quality of life. The more anatomical fracture alignment achieved through 3D printing likely restores normal biomechanics more effectively, facilitating better muscle function and joint articulation [14, 29]. The reduced pain experience, evidenced by lower VAS scores at all postoperative intervals, can be attributed to the even distribution of mechanical loads by the anatomically conforming splint, minimizing pressure points [25]. This enhanced comfort, coupled with a potentially less cumbersome device that allows for better hygiene, likely improved patient adherence to rehabilitation protocols, contributing to the significantly better HSS scores [30]. Future studies might also consider assessing patient-reported outcomes and psychological benefits associated with receiving a customized, high-tech treatment [31].

While this study provides compelling evidence supporting the use of 3D-printed automatic reset splints, several limitations should be acknowledged. First, the retrospective design introduces potential for selection bias despite statistical adjustments for baseline characteristics. Second, the single-center nature of the study may limit generalizability, as surgical expertise and resource availability vary across institutions. Third, the follow-up period of six months, while adequate for assessing initial healing and early functional outcomes, may be insufficient to evaluate long-term complications and functional status, particularly regarding joint degeneration and implant-related issues. Fourth, the cost-effectiveness of this innovative approach was not evaluated in this study; the additional expenses associated with CT scanning, software, and 3D printing equipment must be weighed against the observed clinical benefits in future health economic analyses.

Future research directions should include multicenter randomized controlled trials with longer follow-up periods to confirm these findings and establish generalizability. Economic evaluations are needed to determine the cost-effectiveness of implementing 3D printing technology in orthopedic trauma care. Further technical development should focus on streamlining the design process, reducing production time, and exploring novel materials that might enhance the mechanical and biological properties of these devices. Investigation into the combination of 3D-printed splints with other advanced technologies, such as robotics4 or smart sensors that monitor healing progress, represents another promising avenue for research. Additionally, exploring the application of this technology for more complex fracture patterns or in pediatric populations would help expand its clinical utility.

Conclusion

This study demonstrates that the use of 3D-printed automatic reset splints for the treatment of tibial shaft fractures provides a clinically superior alternative to traditional fluoroscopy-assisted external fixation. The technology offers a multifaceted improvement in patient care by achieving better fracture alignment, accelerating the healing process, reducing the incidence of postoperative complications, enhancing functional recovery of the knee, and improving patient comfort through reduced pain. These benefits are likely attributable to the precision of preoperative virtual planning, the stability afforded by the patient-specific design, and the minimized soft tissue disruption. Despite the promising results, further multi-center studies with longer follow-up are warranted to confirm the long-term benefits and economic viability of this innovative approach. The integration of 3D printing technology represents a meaningful advancement toward personalized and precision medicine in orthopedic trauma care.

Acknowledgements

This study was supported by the Shenzhen Pingshan District Health Bureau and Shenzhen Pingshan District Science and Technology Innovation Bureau (No. 2024121), and the

Shenzhen Science and Technology Program (No. JCYJ20210324111205015).

Disclosure of conflict of interest

None.

Address correspondence to: Aorui Yu, Department of Traditional Chinese Medicine Orthopaedic Manipulation, Shenzhen Pingle Orthopaedic Hospital Affiliated to Guangzhou University of Traditional Chinese Medicine, No. 9 Pingle Road, Pingshan District, Shenzhen 518118, Guangdong, China. E-mail: Yuaorui1986@163.com

References

[1] Turley L, Barry I and Sheehan E. Frequency of complications in intramedullary nailing of open tibial shaft fractures: a systematic review. EFORT Open Rev 2023; 8: 90-99.
[2] Shen M and Tejwani N. Open tibial shaft fracture fixation strategies: intramedullary nailing, external fixation, and plating. OTA Int 2024; 7 Suppl: e316.
[3] Mittlmeier T. Editorial-focus on tibia shaft fractures. Eur J Trauma Emerg Surg 2023; 49: 2327-2328.
[4] Qian S, Shen Y, Sun L and Wang Z. Treatment preferences and current practices regarding open tibial shaft fractures. Front Public Health 2024; 12: 1331654.
[5] Albushtra A, Mohsen AH, Alnozaili KA, Ahmed F, Aljobahi YMAA, Mohammed F and Badheeb M. External fixation as a primary and definitive treatment for complex tibial diaphyseal fractures: an underutilized and efficacious approach. Orthop Res Rev 2024; 16: 75-84.
[6] Hui T, Wang J, Yu Y, Dong H and Lin W. External fixator versus Ilizarov external fixator for pediatric tibial shaft fractures: a retrospective comparative study. Injury 2024; 55: 111376.
[7] Le Baron M, Maman P, Volpi R and Flecher X. External fixation as definitive treatment or external fixation followed by early fixation in open fractures of the tibial shaft: a descriptive study. Injury 2024; 55 Suppl 1: 111477.
[8] Alsharef JF, Ghaddaf AA, AlQuhaibi MS, Shaheen EA, AboAljadiel LH, Alharbi AS, AlHidri BY, Alamri MK and Makhdom AM. External fixation versus intramedullary nailing for the management of open tibial fracture: meta-analysis of randomized controlled trials. Int Orthop 2023; 47: 3077-3097.
[9] O'Connor HA, Adams LW, MacFadden LN and Skelley NW. 3D printed orthopaedic external fixation devices: a systematic review. 3D Print Med 2023; 9: 15.
[10] Kelly C and Adams SB Jr. 3D printing materials and technologies for orthopaedic applications. J Orthop Trauma 2024; 38: S9-S12.
[11] Meng M, Wang J, Huang H, Liu X, Zhang J and Li Z. 3D printing metal implants in orthopedic surgery: methods, applications and future prospects. J Orthop Translat 2023; 42: 94-112.
[12] Liang W, Zhou C, Zhang H, Bai J, Jiang B, Jiang C, Ming W, Zhang H, Long H, Huang X and Zhao J. Recent advances in 3D printing of biodegradable metals for orthopaedic applications. J Biol Eng 2023; 17: 56.
[13] Moldovan F, Gligor A and Bataga T. Integration of three-dimensional technologies in orthopedics: a tool for preoperative planning of tibial plateau fractures. Acta Inform Med 2020; 28: 278-282.
[14] Duan S, Xu R, Liang H, Sun M, Liu H, Zhou X, Wen H and Cai Z. Study on the efficacy of 3D printing technology combined with customized plates for the treatment of complex tibial plateau fractures. J Orthop Surg Res 2024; 19: 562.
[15] Trauma TEWCJCJoO. Guidelines on diagnosis and treatment of open fractures in China (2019). 2019; 21: 921-928.
[16] Kim PH and Leopold SS. In brief: Gustilo-Anderson classification. [corrected]. Clin Orthop Relat Res 2012; 470: 3270-3274.
[17] Müller ME, Nazarian S, Koch P and Schatzker J. The comprehensive classification of fractures of long bones. Springer Science & Business Media, 2012.
[18] Narin S, Unver B, Bakırhan S, Bozan O and Karatosun V. Cross-cultural adaptation, reliability and validity of the Turkish version of the Hospital for Special Surgery (HSS) knee score. Acta Orthop Traumatol Turc 2014; 48: 241-248.
[19] Williamson A and Hoggart B. Pain: a review of three commonly used pain rating scales. J Clin Nurs 2005; 14: 798-804.
[20] Can Kolac U, Paksoy A and Akgün D. Three-dimensional planning, navigation, patient-specific instrumentation and mixed reality in shoulder arthroplasty: a digital orthopedic renaissance. EFORT Open Rev 2024; 9: 517-527.
[21] Shin SH, Kim MS, Yoon DK, Lee JJ and Chung YG. Does a customized 3D printing plate based on virtual reduction facilitate the restoration of original anatomy in fractures? J Pers Med 2022; 12: 927.
[22] Chen Y and Zhang B. 3D printing-assisted total hip arthroplasty and internal fixation for the treatment of fresh acetabular fracture and femoral head necrosis: a case report. Medicine (Baltimore) 2023; 102: e36832.

[23] Bodmer E, Hug U and Liechti R. Comparison of patient-specific implants with standard plates after 3-D-planned corrective osteotomy for distal radial malunions. J Hand Surg Eur Vol 2025; 50: 464-471.
[24] Li H, Li D, Qiao F, Tang L and Han Q. 3D printing adjustable stiffness external fixator for mechanically stimulated healing of tibial fractures. Biomed Res Int 2021; 2021: 8539416.
[25] Qiao F, Li D, Jin Z, Hao D, Liao Y and Gong S. A novel combination of computer-assisted reduction technique and three dimensional printed patient-specific external fixator for treatment of tibial fractures. Int Orthop 2016; 40: 835-841.
[26] Liu X, Gaihre B, Park S, Li L, Dashtdar B, Astudillo Potes MD, Terzic A, Elder BD and Lu L. 3D-printed scaffolds with 2D hetero-nanostructures and immunomodulatory cytokines provide pro-healing microenvironment for enhanced bone regeneration. Bioact Mater 2023; 27: 216-230.
[27] Xiao L, Tang P, Yang S, Su J, Ma W, Tan H, Zhu Y, Xiao W, Wen T, Li Y, Liu S and Deng Z. Comparing the efficacy of 3D-printing-assisted surgery with traditional surgical treatment of fracture: an umbrella review. J Orthop Traumatol 2025; 26: 3.
[28] Jiang L, Li H and Huang L. The efficacy of 3D printing model in the intraarticular osteotomy in the treatment of malunion of tibial plateau fracture. Orthop Surg 2023; 15: 85-92.
[29] Zheng W, Chen C, Zhang C, Tao Z and Cai L. The feasibility of 3D printing technology on the treatment of pilon fracture and its effect on doctor-patient communication. Biomed Res Int 2018; 2018: 8054698.
[30] Zhu B, Xue K, Cai B and Fang J. Evaluating the outcomes of three dimensional printing-assisted osteotomy on treating varus knee deformity from old tibial plateau fractures. Int Orthop 2025; 49: 429-435.
[31] Hu H and Yang H. Impact of 3D printing technology-assisted rehabilitation cycles on prognostic motility in surgically treated tibial plateau fractures: a meta-analysis. Altern Ther Health Med 2024; [Epub ahead of print].